

Transfer CLIP for Generalizable Image Denoising

Jun Cheng, Dong Liang, Shan Tan*

Huazhong University of Science and Technology, Wuhan, China

{jcheng24, liangdong, shantan}@hust.edu.cn

Abstract

Image denoising is a fundamental task in computer vision. While prevailing deep learning-based supervised and self-supervised methods have excelled in eliminating in-distribution noise, their susceptibility to out-of-distribution (OOD) noise remains a significant challenge. The recent emergence of contrastive language-image pre-training (CLIP) model has showcased exceptional capabilities in open-world image recognition and segmentation. Yet, the potential for leveraging CLIP to enhance the robustness of low-level tasks remains largely unexplored. This paper uncovers that certain dense features extracted from the frozen ResNet image encoder of CLIP exhibit distortion-invariant and content-related properties, which are highly desirable for generalizable denoising. Leveraging these properties, we devise an asymmetrical encoder-decoder denoising network, which incorporates dense features including the noisy image and its multi-scale features from the frozen ResNet encoder of CLIP into a learnable image decoder to achieve generalizable denoising. The progressive feature augmentation strategy is further proposed to mitigate feature overfitting and improve the robustness of the learnable decoder. Extensive experiments and comparisons conducted across diverse OOD noises, including synthetic noise, real-world sRGB noise, and low-dose CT image noise, demonstrate the superior generalization ability of our method.

1. Introduction

Image denoising is a significant task in computer vision and image processing. Current supervised denoising methods leveraging powerful deep neural networks and large-scale datasets have achieved exceptional performance in both synthetic and real-world noise removal [33, 60]. However, these supervised denoisers tend to overfit the noise present in the training datasets, resulting in poor generalization to out-of-distribution (OOD) noise [6]. On the other hand, unsupervised and self-supervised denoising methods

[12, 18, 26, 28, 44, 54] directly focus on the target domain in which the target noisy images reside and hence bypass OOD generalization. Nevertheless, these methods are inherently vulnerable to unseen noise [7] and the collection of target noisy datasets is not always available. Therefore, it is critical to enhance the generalization of deep denoisers.

OOD generalization has been popular research in high-level vision tasks like image recognition and segmentation [51, 70]. In contrast, attention to OOD generalization within image denoising is limited. Existing research in this area primarily consists of two aspects: generalization across degradation levels and generalization across degradation types. Regarding the former, some works trained blind denoisers [18, 60, 62] or bias-free networks [41, 63] to handle noise with varying levels. However, these methods are confined to specific noise and cannot generalize to unseen noise types. For the latter, several works aimed to fortify models against general OOD noise. Particularly, MaskDenoising [6] incorporated dropout units into the model training to enforce the denoiser to learn the reconstruction of image contents. DIL [32] built upon causality and meta-learning and encouraged the model to learn distortion-invariant representations. HAT [58] designed an adversarial attack for deep denoisers and then conducted adversarial training.

Recently, through solving the image-text alignment problem based on hyper-scale datasets, the contrastive language-image pre-training (CLIP) model [48] has demonstrated remarkable generalization capacity in downstream open-world image recognition tasks. A series of extensions on CLIP through frozen models [65, 69], model fine-tuning [49], visual prompts [71], distillations [19, 31], and so on [34] have been proposed to transfer the generalization ability of CLIP from classification to dense prediction tasks, including open-vocabulary segmentation [34] and zero-shot depth estimation [65]. However, the feasibility of CLIP for robust restoration in low-level tasks remains unexplored. We therefore ask, is CLIP robust to image noise and can we transfer it for generalizable image denoising?

In this paper, we find that the dense feature maps from the frozen ResNet image encoder of CLIP within specific scales exhibit remarkable resilience to noise, a property that

*Corresponding author.

is not easy to obtain via supervised learning. These features of clean images and their noisy counterparts show significant similarities in terms of cosine and CKA [25] similarity measures. In addition, these features maintain a clear distinction for images with different contents and semantics. Such distortion-invariant and content-related properties are desirable for generalizable denoising as the robust and distinctive features commendably represent the latent image regardless of the corruption in the noisy measurement. As a result, we propose an asymmetrical encoder-decoder denoising network by integrating the frozen ResNet image encoder of CLIP and a learnable image decoder. The multi-scale features of noisy images from the frozen encoder, as well as an extra dense feature represented by the noisy image, are progressively incorporated into the decoder to recover high-quality images. Through supervised training on a single noise type and noise level, the proposed concise denoiser, termed CLIPDenoising, exhibits good generalization capacity to various OOD noises.

By employing the frozen image encoder, the image denoising task turns into recovering clean images from fixed features. During training, the inherent similarity of training images [5] as well as their respective dense features will inevitably affect feature diversity, leading to potential feature overfitting. Therefore, we propose progressive feature augmentation to randomly perturb these features from the frozen CLIP with increasing randomness at deeper scales. In total, our contributions are summarized as follows:

- We identify that dense features from the frozen ResNet encoder of CLIP possess distortion-invariant and content-related properties. Leveraging this finding, we incorporate these features along with the noisy image into a learnable image decoder to construct a generalizable denoiser.
- We propose the progressive feature augmentation strategy to further improve the robustness of our approach.
- To the best of our knowledge, we are the first to utilize CLIP for generalizable denoising. Extensive experiments and comparisons on various OOD noises, including synthetic noise, real-world sRGB noise, and low-dose CT noise, demonstrate superior generalization of our method.

2. Related works

2.1. Deep Learning-based Image Denoising

Supervised denoising methods generally build upon powerful deep architectures (e.g., CNNs [62, 63], non-local networks [66], and Transformer [33, 35, 60]), large-scale paired datasets (e.g., SIDD [1]), and diverse optimization targets (e.g., L1/L2 losses [67], adversarial loss [27] or diffusion loss [50]) and have achieved state-of-the-art performance. However, the strong reliance on paired datasets and *i.i.d.* assumption makes them vulnerable to unseen and OOD noise [6]. To circumvent this limitation, many unsu-

pervised and self-supervised denoising methods [4, 12, 18, 23, 26, 28, 44, 46, 54] have been introduced to directly handle the target noisy images. While effective, these methods bypass tackling the generalization problem, leading to insufficient improvement in the OOD robustness of deep denoisers. Consequently, there remains a significant gap in research concerning generalizable denoising.

2.2. OOD Generalization in Image Denoising

Existing research on generalizable image denoising primarily consists of generalization across degradation levels and generalization across degradation types. The former addresses known noise types at unknown levels during inference, while the latter strives for general OOD robustness. Regarding the former, DnCNN [62] proposed to train blind denoisers, which are capable of handling specific noise types with varying levels. Mohan et al. [41] discovered that bias-free (BF) denoisers trained on limited noise ranges exhibited robustness to unseen noise levels. Consequently, the BF architecture was adopted in subsequent models like DRUNet [63] and Restormer [60]. Regarding the latter, GainTuning [42] employed a test-time training strategy to optimize the denoiser for each noisy input. Chen et al. [7] disentangled latent clean features from multiple corrupted versions of the same image to achieve OOD generalization. MaskDenoising [6] revisited the commonly employed dropout operation in high-level vision tasks and integrated these units into model training. DIL [32] combined counterfactual distortion augmentation and meta learning-based optimization to develop a generalizable restoration network. HAT [58] incorporated the adversarial attack and adversarial training to improve the OOD generalization of deep denoisers. Despite these advancements, there remains room for further improvement in generalizability.

2.3. CLIP-based Generalization

CLIP has demonstrated remarkable generalization abilities in open-world image recognition [48]. Subsequent works, such as MaskCLIP [69], DenseCLIP [49], ZegCLIP [71], and others [34, 38], extended CLIP to dense prediction tasks, enabling zero-shot or open-vocabulary image segmentation. There are also studies explicitly distilling CLIP while maintaining its zero-shot performance [19, 31, 55]. Nevertheless, due to a distinct domain gap, there remains a lack of research on harnessing CLIP’s exceptional generalization capacity for low-level vision tasks. This gap in exploration serves as a primary motivation for our work.

2.4. Foundation Models for Image Restoration

Utilizing foundation models to solve domain-specific tasks has become prevalent in computer vision. Similar to high-level vision tasks, many works have integrated large pre-trained models for image restoration. Diffusion model

stands as a state-of-the-art generation method and many papers have leveraged the pre-learned diffusion priors to address various image restoration tasks [9, 13, 21, 22, 72]. Regarding Segment Anything model [24], some works have integrated it into image deblurring [30], image dehazing [20], and super-resolution [37, 56]. Yu et al. [59] introduced the semantic pyramid auto-encoder to enable large language models to perform image deblurring and inpainting. Additionally, Luo et al. [39] leveraged CLIP to predict high-quality image features and degradation features, subsequently integrating them into the image restoration model for universal image restoration. While existing works predominantly concentrate on leveraging foundation models to enhance image restoration performance, our paper aims to emphasize the enhancement of OOD generalization ability.

3. Method

In this section, we first check whether CLIP that has been trained on hyper-scale image-text datasets enjoys some good properties for generalizable denoising. Based on the analysis in Section 3.1, we propose the simple and generalizable denoiser in Section 3.2, followed by the strategy of progressive feature augmentation in Section 3.3.

3.1. Analyzing Features of CLIP Image Encoder

CLIP offers two variants of image encoders, i.e., ResNet [16] and ViT [11]. The ResNet version extracts multi-scale feature maps through sequential Conv-blocks and Pooling operations, while the ViT version breaks down images into smaller 16×16 patches and then employs standard Transformer operations. For deep learning-based image denoising, low-level image details and textures are critical for reconstructing high-quality images [61]. Existing methods utilize either the *single-scale* pipeline [33, 35] or the *encoder-decoder* architecture with skip connections [60, 63] to preserve spatial details. As the ViT architecture directly processes overly downsampled image features, it abandons spatial image details and hence is not suitable for image denoising. Consequently, we focus on analyzing and utilizing the ResNet for our further analysis and method.

Distortion-invariant property. We examine the dense feature maps before each (average or attention)-pooling operation in the CLIP ResNet image encoder. (Refer Alg. 1 in the Supplementary Material for details). This yields a total of five multi-scale features, denoted as $\mathbf{F}^1 \in \mathbb{R}^{\frac{H}{2} \times \frac{W}{2} \times C}$ and $\mathbf{F}^i \in \mathbb{R}^{\frac{H}{2^i} \times \frac{W}{2^i} \times 2^i C}$, $i \in \{2, \dots, 5\}$, where $H \times W$ are the spatial dimensions of the input image, and C is the base channel number. To assess the robustness of these features, we start with a clean image \mathcal{I}_c and introduce diverse *i.i.d.* Gaussian noises to create corresponding noisy images \mathcal{I}_n . Note that the image intensity range used in this section is $[0, 1]$. The clean image features \mathbf{F}_c^i and the noisy image features \mathbf{F}_n^i are obtained by passing both the high-quality

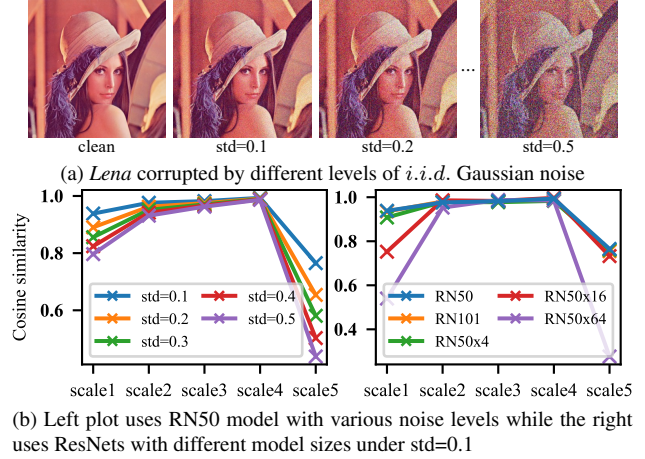


Figure 1. Feature similarity analysis of the CLIP ResNet image encoder for image *Lena*. Cosine similarity between \mathbf{F}_c^i and \mathbf{F}_n^i with regard to different noise levels and model sizes is displayed

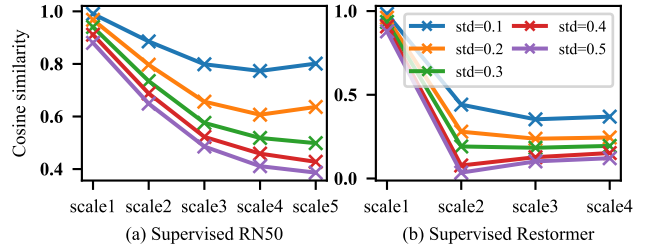


Figure 2. Feature similarity analysis of ResNet50 (supervised training for image classification, not from CLIP) and Restormer (supervised training for blind Gaussian noise removal)

and degraded images through the frozen ResNet. Subsequently, the cosine similarity between \mathbf{F}_c^i and \mathbf{F}_n^i is computed at each scale i . We show the result in Fig. 1, where five distinct noise levels and five pre-trained ResNets with increasing sizes (i.e., more residual blocks within each scale of ResNet) provided by CLIP are considered.

From Fig. 1, we observe that the initial *four* features \mathbf{F}_n^i from the RN50, under various corruption levels, show significant similarities to their corresponding \mathbf{F}_c^i , with higher similarity at deeper scales i . On the other hand, as the model size increases, the resemblance between \mathbf{F}_c^1 and \mathbf{F}_n^1 dramatically decreases even under smaller $\text{std}=0.1$. Additional results using *CKA similarity* metric [25], *Poisson degradation*, and *other image* are given in Figs. 9, 10, 11 in the Supplementary Material, which all suggest similar observations. From these findings, we conclude that features $\mathbf{F}_n^i, i \in \{1, \dots, 4\}$ from CLIP frozen RN50 are robust and distortion-invariant, which is essential for building generalizable denoisers. Additionally, we contrast these findings with feature analyses of ResNet50 trained on ImageNet for supervised image classification and Restormer trained on *i.i.d.* Gaussian noise with $\sigma \in [0, 0.2]$ for blind denoising,

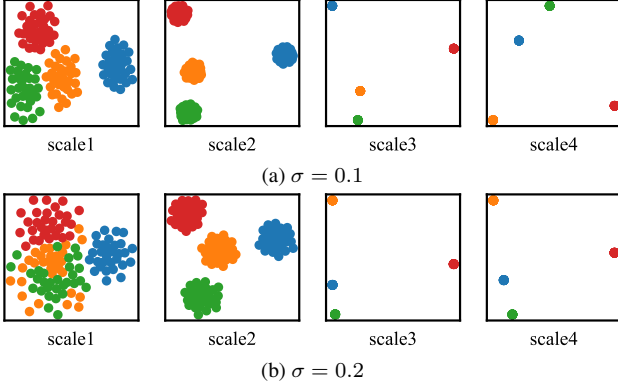


Figure 3. The t-SNE plots of $\mathbf{F}_n^i, i \in \{1, \dots, 4\}$ from four corrupted images with diverse contents, i.e., *Lena*, *Baboon*, *F16* and *Peppers* from set9 [10] under *i.i.d.* Gaussian noise with two noise levels. Different colors denote features of different images

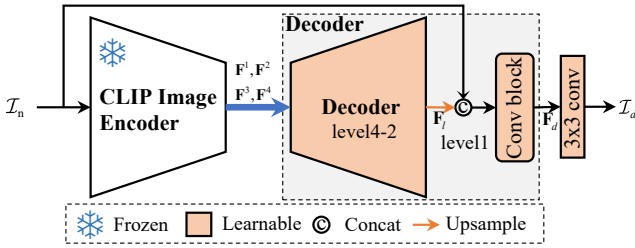


Figure 4. The CLIPDenosing for generalizable image denoising, which comprises the frozen RN50 encoder from CLIP, a learnable image decoder, and 3×3 convolution

and report the results in Fig. 2. The distinction between Fig. 1 and Fig. 2 underlines that such distortion-invariant property is not universal and originates from CLIP. We present a brief discussion in Section 5 about why the RN50 image encoder of CLIP holds this appealing property.

Content-related property. We then check whether the above features from CLIP frozen RN50 are content-related, that is, if features of two noisy images with distinctive contents are different. Given M distinctive clean images $\mathcal{I}_c^m, m \in \{1, \dots, M\}$, we generate multiple noisy images \mathcal{I}_n^m from $\mathcal{N}(\mathcal{I}_c^m, \sigma^2 I)$ and obtain the corresponding multi-scale features $\mathbf{F}_n^i, i \in \{1, \dots, 4\}$ from the frozen RN50. We then compute the two-dimensional embeddings of these features using the t-SNE method [53] and present the result in Fig. 3. We find that the low-dimensional representation of \mathbf{F}_n^i from different noisy image \mathcal{I}_n^m showcases clear separation under different scale i and noise level σ , indicating a strong correlation between the image content and their multi-scale features from CLIP RN50.

3.2. Building a Generalizable Denoiser

Leveraging the favorable attributes of the frozen RN50 encoder from CLIP, we established a simple, effective, and

generalizable denoiser, of which the architecture is depicted in Fig. 4. Our model mainly consists of the frozen RN50 image encoder and a 4-level learnable image decoder. Given the noisy input $\mathcal{I}_n \in \mathbb{R}^{H \times W \times 3}$, the multi-scale features $\mathbf{F}_n^i, i \in \{1, \dots, 4\}$ from the frozen RN50 are first extracted. The decoder takes \mathbf{F}_n^4 as input and progressively recovers the high-resolution features. During the up-sampling, $\mathbf{F}_n^i, i \in \{1, 2, 3\}$ are concatenated with the decoder features to incorporate the multi-scale feature information into the restoration (level-4 to -2). Subsequently, the decoder at level-2 outputs the feature $\mathbf{F}_l \in \mathbb{R}^{\frac{H}{2} \times \frac{W}{2} \times C}$. At level-1, \mathbf{F}_l is then upsampled and concatenated with the noisy input \mathcal{I}_n , producing $\mathbf{F}_d \in \mathbb{R}^{H \times W \times C}$ after a final Conv-block. Ultimately, the denoised image \mathcal{I}_d is obtained through a 3×3 convolution operation applied on \mathbf{F}_d . The learnable decoder, devised to align with the ResNet encoder, is convolution-based and comprises multiple Conv-ReLU-Conv-ReLU sequences. More details about the decoder are given in the Supplementary Material. It’s worth noting that the model incorporates the noisy image \mathcal{I}_n as an additional image feature into the decoder, which is important and reasonable as the noisy image \mathcal{I}_n itself contains rich image details and can be considered as one distinctive dense feature. This operation will be analyzed further in Section 4.5.

During the training, we synthesize \mathcal{I}_n from \mathcal{I}_c based on a fixed noise type and level, and optimize the loss function,

$$\mathcal{L} = \mathbb{E}_{p(\mathcal{I}_c)} \|\mathcal{I}_d - \mathcal{I}_c\|_1 \quad (1)$$

Note that, we do not employ global residual learning as we aim to restore the high-quality image from its robust features rather than restore the residual noise. In inference, we directly evaluate our model on OOD noise. Ablations in Section 4.5 indicate that our simple baseline, i.e., CLIPDenosing, has already achieved good generalizability.

3.3. Progressive Feature Augmentation

By utilizing the frozen CLIP RN50 as the image encoder, the image denoising task turns into mapping invariant features to high-quality images. However, as images in the training dataset naturally exhibit certain degrees of similarities (e.g., similar textures in different images), the corresponding multi-scale features from CLIP RN50 tend to follow these similarities. This will reduce the feature diversity and can potentially lead to feature overfitting problems. To avoid this issue and enhance the decoder’s robustness, we introduce the strategy of progressive feature augmentation, inspired by [29]. During the training phase, we apply random perturbations to the multi-scale features \mathbf{F}^i as follows

$$\hat{\mathbf{F}}^i = \alpha_i \odot \mathbf{F}^i, \alpha_i \sim \mathcal{N}(\mathbf{1}, (\gamma \times i)^2 I), i \in \{1, \dots, 4\} \quad (2)$$

where \odot denotes the element-wise multiplication and α_i has the same size as \mathbf{F}^i .

In Eq. (2), α_i is sampled from the *i.i.d.* Gaussian distribution with mean one and std $\gamma \times i$. For larger i , we inject more randomness to \mathbf{F}^i as the deeper features tend to capture more semantic information and should also be more robust; Regarding smaller i , we inject less noise to preserve texture- and detail-related information contained in the shallow features. We note that such progressive feature augmentation is simple but effective.

4. Experiments

In this section, we first introduce experimental settings of denoising diverse OOD noises. Quantitative and qualitative results of our method and comparisons with other methods are then presented. The ablation is conducted in the last.

4.1. Experimental Settings

Synthetic noise. We choose *i.i.d.* Gaussian noise with $\sigma = 15$ as the in-distribution noise and consider 5 kinds of synthetic OOD noise: (1) *i.i.d.* Gaussian noise with $\sigma \in \{25, 50\}$, (2) spatial Gaussian noise with $\sigma \in \{45, 50, 55\}$, (3) Poisson noise with levels $\alpha \in \{2.5, 3, 3.5\}$, (4) Speckle noise with levels $\sigma^2 \in \{0.02, 0.03, 0.04\}$ and (5) Salt&Pepper noise with levels $d \in \{0.012, 0.016, 0.02\}$. We follow MaskDenoising [6] to generate these OOD noises and adopt Kodak24 [14], McMaster [64], CBSD68 [40], and Urban100 [17] as test sets. Note that Gaussian and spatial Gaussian noises are generated in the intensity range of $[0, 255]$ while the rest uses the intensity range of $[0, 1]$, so as to be consistent with MaskDenoising.

Regarding the implementation details of our method, we build on CBSD432 dataset [40] and synthesize noisy images using *i.i.d.* Gaussian noise with $\sigma = 15$ in the online fashion. Supervised training based on Eq. (1) and Fig. 4 is conducted. In the training phase, we utilize the AdamW [36] optimizer combined with the cosine-annealing learning rate. We conduct 300k training iterations with a batch size of 16, and the learning rate decreases from an initial value of $3e^{-4}$ to a final value of $1e^{-6}$. The training patch size is 128×128 and random geometric augmentations are applied to training patches. We set $\gamma = 0.025$ to augment the dense features from frozen RN50 of CLIP. We perform all experiments using PyTorch [47] and an Nvidia 2080ti GPU. Peak signal-to-noise ratio (PSNR) and structural similarity (SSIM) metrics are used to evaluate the denoising quality.

Real-world sRGB noise. For real-world sRGB noise, we consider SIDD validation dataset [1], PolyU [57] and CC [43] as test sets. These datasets comprise natural noisy sRGB images from smartphones and commercial cameras. During training, we simulate sRGB noise based on DIV2K dataset [2] and the image signal processing pipeline, following CBDNet [15]. In particular, we use a fixed level of Poisson-Gaussian noise, i.e., $\sigma_s = 0.04, \sigma_c = 0.03$ in the raw domain to generate noisy images in order to accentuate

the distribution gap of data between training and testing. The optimization here is identical to that of synthetic noise.

Low-dose CT image noise. We utilize CLIPDenoising trained on *i.i.d.* Gaussian noise to remove real-world low-dose (LD) CT image noise, which is known to be complex and hard to model [12]. We use AAPM-Mayo Clinic Low Dose CT Grand Challenge dataset [3], which provides 1mm thickness abdomen slices with quarter-dose images (noisy) and corresponding normal-dose (ND) images (GT). We select 5410 NDCT images from nine patients combined with *i.i.d.* Gaussian noise with $\sigma = 5$ for training and use 526 LDCT images from patient L506 for test. To accommodate the one-channel CT image, we insert a learnable 1×1 convolution ahead of the CLIP RN50 encoder, which converts the single-channel image into a three-channel image. The optimization details remain the same as the above except that we set the total training iterations to 40k in this case.

4.2. Synthetic Noise Removal

Compared methods. We compare our method against three representative works on generalizable denoising, i.e., MaskDenoising [6], DIL [32], and HAT [58]. For MaskDenoising, we use the officially trained model. Regarding DIL and HAT, we follow their source codes and experimental settings to train denoisers based on *i.i.d.* Gaussian noise with $\sigma \in \{5, 10, 15, 20\}$ and $\sigma \in [0, 25]$, respectively. Note that *multiple noise levels* are required by these two methods during the training phase to achieve generalization. We additionally evaluate DnCNN [62] and Restormer [60] trained on *i.i.d.* Gaussian noise with $\sigma = 15$.

Results. We present comprehensive quantitative comparisons of various methods across diverse noise types, levels, and datasets in Table 1 and Table 9 (in the Supplementary Material). As indicated by Tables 1 and 9, our CLIPDenoising exhibits commendable in-distribution performance while demonstrating remarkable robustness against all considered OOD noises. In comparison, the compared methods merely excel in some specific noise types.

As shown in the first part of Table 9, Restormer achieves commendable performance in in-distribution noise. However, it struggles in tackling unseen noise levels and types (see Tables 1 and 9), indicating the overfitting to the noise in the training set. Compared with Restormer, DnCNN has a weaker modeling capacity but shows better robustness to OOD noise, which however is significantly behind the methods specialized in generalizable denoising. In comparisons among MaskDenoising, DIL, HAT, and CLIPDenoising, DIL and our method stand out as the only effective methods in eliminating Gaussian noise with higher noise level, i.e., $\sigma = 50$, and our method surpasses DIL in average as indicated in Table 1. Regarding unseen noise types, MaskDenoising outperforms HAT and DIL in spatial Gaussian noise; Conversely, HAT and DIL exhibit notable advan-

Table 1. Quantitative comparison (PSNR/SSIM) of different methods on CBSD68, McMaster, Kodak24 and Urban100 datasets with regard to diverse synthetic OOD noises. The best results are highlighted in **bold** and the second best is underlined. Note that *multiple noise levels* are required by HAT and DIL during the training to achieve generalization, while our method only needs *one noise level* for training

Noise Types	Datasets	DnCNN [62]	Restormer [60]	MaskDenoising [6]	HAT [58]	DIL [32]	Ours
Gauss $\sigma = 50$	CBSD68	19.84/0.363	19.92/0.365	20.68/0.432	20.95/0.441	26.43/0.717	26.69/0.731
	McMaster	20.18/0.312	20.47/0.312	20.63/0.379	20.79/0.364	<u>26.61/0.669</u>	27.43/0.727
	Kodak24	19.78/0.301	20.12/0.321	20.72/0.368	21.04/0.390	27.46/0.736	<u>27.39/0.723</u>
	Urban100	19.62/0.420	19.36/0.437	20.51/0.485	20.80/0.492	<u>25.89/0.768</u>	26.27/0.769
Spatial Gauss $\sigma = 55$	CBSD68	25.91/0.699	23.51/0.595	<u>26.72/0.762</u>	26.39/0.713	24.61/0.630	27.60/0.797
	McMaster	26.18/0.649	24.01/0.539	<u>26.89/0.709</u>	26.62/0.665	24.82/0.574	28.31/0.775
	Kodak24	25.98/0.653	22.99/0.533	<u>27.28/0.745</u>	26.40/0.671	24.56/0.572	28.29/0.786
	Urban100	25.55/0.727	24.13/0.660	26.10/0.788	<u>26.48/0.742</u>	24.80/0.673	27.68/0.822
Poisson $\alpha = 3.5$	CBSD68	24.37/0.627	22.20/0.559	24.24/0.638	26.61/0.733	<u>27.64/0.819</u>	27.67/0.818
	McMaster	25.50/0.651	21.93/0.579	25.17/0.590	27.54/0.723	28.91/0.825	<u>28.81/0.820</u>
	Kodak24	24.49/0.560	22.55/0.517	24.30/0.572	27.10/0.695	28.60/0.821	28.66/0.813
	Urban100	23.57/0.649	21.08/0.584	23.90/0.669	25.95/0.746	<u>27.12/0.854</u>	27.15/0.838
Salt&Pepper $d = 0.02$	CBSD68	26.53/0.746	23.59/0.679	<u>29.74/0.843</u>	27.55/0.782	29.45/0.822	29.81/0.844
	McMaster	25.72/0.691	23.05/0.640	<u>29.28/0.773</u>	26.62/0.727	<u>29.28/0.773</u>	29.79/0.807
	Kodak24	27.10/0.723	23.81/0.639	<u>30.56/0.842</u>	28.19/0.766	29.99/0.810	30.61/0.837
	Urban100	25.61/0.777	23.51/0.734	28.43/0.861	26.88/0.792	<u>29.21/0.841</u>	29.40/0.869

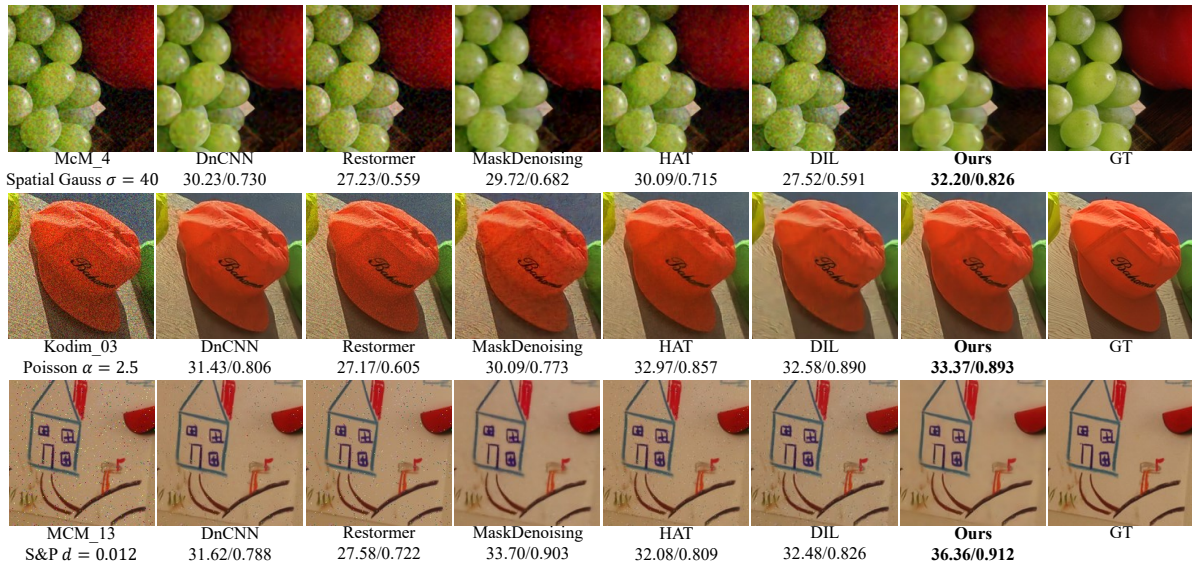


Figure 5. Qualitative denoising results on synthetic OOD noise. During the training, all the methods do not encounter the test noise types. PSNR/SSIM values are listed underneath the respective images. Zoom-in for a better comparison

tags over MaskDenoising in handling Poisson and Speckle noise. In contrast, our method demonstrates consistent and competitive performance across all types of OOD noise, suggesting the great benefits from the superior distortion-invariant property of the frozen CLIP ResNet encoder.

Note that our method, though exhibiting slightly lower performance than HAT and DIL in dealing with Speckle noise (see the middle part of Table 9), is accomplished with just one noise level, unlike these methods which necessitate multiple noise levels during training. Fig. 5 and Figs. 14, 15 (in the Supplementary Material) present the qualitative comparison among various methods. These visual results indicate that our method can effectively denoise OOD noise while preserving image contents and details.

4.3. Real-world sRGB Noise Removal

Compared methods. We again consider MaskDenoising, DIL, and HAT for comparison. We train MaskDenoising and DIL using their respective source codes with the same synthetic sRGB dataset used in our method. DIL mandates that the training set is categorized into four groups based on Bayer patterns. As for HAT, it’s implemented based on the clean DIV2K dataset with *i.i.d.* Gaussian noise within the range of $\sigma \in [0, 50]$ to ensure its standard functionality. In addition, we also consider two unsupervised denoising methods, i.e., CVF-SID [44] and LUD-VAE [68], which necessitate real-world noisy images for training.

Results. We present quantitative and qualitative results of different methods on real-world noise removal in Ta-



Figure 6. Qualitative results on real-world sRGB noise. PSNR/SSIM values are listed underneath the respective images.

Table 2. Quantitative comparison (PSNR/SSIM) of different methods on real-world sRGB datasets, i.e., SIDD Val, PolyU, and CC.

Methods	SIDD Val	PolyU	CC
MaskDenoising [6]	33.14/0.913	24.78/0.812	25.63/0.881
HAT [58]	28.58/0.570	37.25/0.948	35.27/0.901
DIL [32]	34.76/0.848	37.65/0.959	36.10/0.948
Ours	34.79/0.866	37.54/0.960	36.30/0.941
CVF-SID [44]	34.81/0.944	35.86/0.937	33.29/0.913
LUD-VAE [68]	34.91/0.892	36.99/0.955	35.48/0.941

ble 2, Fig. 6 and Fig. 16 (in the Supplementary Material), respectively. It is clear from Table 2 that our method nearly achieves the best performance among the methods of generalizable denoising. Notably, DIL stands on par with our CLIPDenoising, although it requires constructing *four distinct confounders*, i.e., four distortions during training, while our method does not have this requirement. In addition, compared with CVF-SID and LUD-VAE, our method shows competitive results on SIDD dataset and outperforms them on PolyU and CC datasets. As our method does not rely on real-world datasets, it emerges as a more practical and universal alternative compared to those noisy datasets-based unsupervised methods. The visual comparisons in Figs. 6 and 16 further underline the effectiveness of CLIP-Denoising in addressing real-world sRGB noise.

4.4. Low-dose CT Image Noise Removal

Compared methods. We compare our method against the representative works in LDCT image denoising, namely Noise2Sim [45] and ScoreSDE-CT [52]. Noise2Sim relies on the adjacent and similar LDCT images to train the denoiser, while ScoreSDE-CT learns score priors from NDCT images based on ScoreSDE and subsequently conducts posterior sampling for LDCT images. For both methods, we use their official codes and the same dataset as ours.

Results. We show the quantitative outcomes in Table 3 and the denoised images in Fig. 7. Our method outperforms ScoreSDE and achieves comparable performance to Noise2Sim, indicating the effectiveness of the robust CLIP

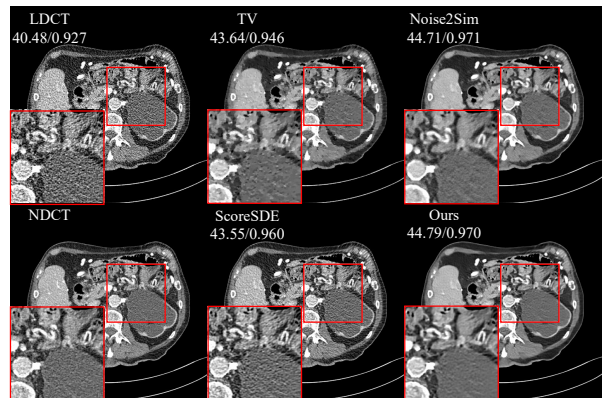


Figure 7. Denoising results on LDCT image. PSNR/SSIM are listed on the respective images. Display window: [-160, 240]HU.

Table 3. Quantitative comparison of different methods on low-dose CT abdomen slices. Note that Noise2Sim requires *adjacent LDCT images* for training, while we only demand *NDCT images*

TV	ScoreSDE [52]	Noise2Sim [45]	Ours
44.81/0.972	45.36/0.972	45.98/0.978	<u>45.88/0.976</u>

RN50 encoder in CT images. This holds substantial appeal as it enables direct knowledge transfer from models trained on natural images to medical domains, eliminating the need for, e.g., numerous adjacent low-dose CT images in Noise2Sim, especially beneficial in clinical scenarios.

4.5. Ablations

Here, we conduct ablation studies on synthetic noise to better evaluate the performance of our method.

Ablation on the use of noisy image and F^5 . Our model utilizes the noisy input as an extra dense feature to facilitate the transfer of image details and structures for restoration. Removing this operation significantly impacts the model’s performance, as shown in the third row of Table 4. Without integrating the noisy image \mathcal{I}_n into the decoder, the model’s performance drastically declines, in both in-distribution and OOD cases. This highlights that although the dense features

Table 4. Effects of using the input image \mathcal{I}_n , features \mathbf{F}^5 , different training types and progressive feature augmentation on synthetic OOD noise removal under Kodak24 dataset

	Gauss $\sigma = 15$	Gauss $\sigma = 50$	Speckle $\sigma^2 = 0.04$
Baseline	34.69/0.922	26.87/0.692	30.60/0.871
w/o input \mathcal{I}_n	30.37/0.888	21.76/0.413	26.93/0.761
+ feature \mathbf{F}^5	34.03/0.916	25.61/0.645	30.39/0.865
+ <i>random</i>	34.89/0.925	20.87/0.342	29.61/0.821
+ <i>finetune</i>	34.91/0.926	19.03/0.276	27.37/0.694
+ PFA	34.69/0.922	27.39/0.723	30.67/0.876

Table 5. Effects of using different CLIP ResNet versions on synthetic OOD noise under Urban100 dataset (without PFA)

	Gauss $\sigma = 50$	Poisson $\alpha = 3.5$	Speckle $\sigma^2 = 0.04$
RN50	25.86/0.743	27.11/0.837	28.61/0.871
RN50x4	24.04/0.651	26.31/0.809	28.40/0.869
RN50x16	23.44/0.731	22.26/0.762	18.95/0.707

from the frozen CLIP RN50 exhibit favorable properties, they lack crucial details of the input image, rendering them ineffective for standalone restoration. In addition, utilizing feature \mathbf{F}^5 , which does not hold distortion-invariant property as identified in Section 3.1, also leads to a decline in both in-distribution and OOD performance.

Ablation on training types. We evaluate two optional training types to optimize our model: (1) *random*, where the image encoder is randomly initialized and the entire network is trained from scratch, and (2) *finetune*, which initializes the image encoder using the pre-trained RN50 from CLIP and then finetunes the complete model. As observed in Table 4, both training types improve the in-distribution denoising performance since the denoiser begins to overfit the training noise. Consequently, the resultant models show poor robustness to OOD noise (also see Fig. 8) as the original property of the frozen RN50 has been broken.

Ablation on progressive feature augmentation (PFA). The inclusion of progressive feature augmentation is highlighted in the last row of Table 4. This strategy does not affect in-distribution performance but enhances the model’s generalization to OOD noise, demonstrating its efficacy.

Ablation on ResNet versions. In Section 3.1, we observe that the first feature \mathbf{F}^1 from larger ResNet models of CLIP does not hold the distortion-invariant property. Here we ablate its effect on the generalization ability. We substitute the frozen RN50 model in Fig. 4 with frozen RN50x4 and RN50x16, respectively, and then train the corresponding denoisers. The outcomes, as depicted in Table 5, clearly indicate a substantial reduction in the generalization ability of denoisers under frozen RN50x4 and RN50x16. This underscores the significance of robust shallow features for achieving generalizable denoising.

More experiments on the computational cost (Table 6) and image deraining (Table 7) are provided in the supp.

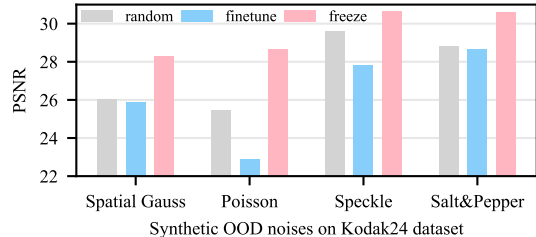


Figure 8. Robustness of *random*, *finetune* and *freeze* (ours) to diverse OOD noises. Here, the highest OOD noise levels are used.

5. Discussions and Limitations

Why are dense features of CLIP RN50 encoder robust to noise? During the training of the CLIP model, the dense features of the CLIP image decoder might overlook high-frequency information within images, including noise and fine textures. Instead, they tend to prioritize image contents to align more effectively with text semantics. This hypothesis is reasonable as the text cannot provide dense and high-frequency details for images.

Is the robust property unique to CLIP RN50? We hypothesize that other well-established self-supervised representation learning may induce a similar property as CLIP. To validate this, we perform feature analysis and OOD experiments using the frozen RN50 pre-trained by MoCo-v3 [8], a prominent self-supervised pre-training method. The findings presented in Fig. 13 and Table 10 (in the Supplementary Material) suggest that a denoiser based on MoCo-v3 RN50 also exhibits a certain level of OOD robustness.

Transformer architectures for the denoiser. As discussed in Section 3.1 and verified in Table 8 of the supp, the CLIP ViT image encoder excessively downsamples image features, rendering it unsuitable for image restoration. We also attempt to implement a Transformer-based decoder by replacing the Conv-block with the Restormer-block. However, the resultant denoiser tends to overfit the training noise, leading to a decrease in its generalization. Additional strategies are needed to mitigate this overfitting.

6. Conclusion

This paper introduces a simple yet robust denoiser that can generalize to various OOD noises. Our method builds upon the discovery that the first four multi-scale dense features from CLIP frozen RN50 are distortion-invariant and content-related. By integrating these features and the noisy input image into the learnable image decoder, we construct a denoiser with generalization capabilities. Comprehensive experiments and comparisons on diverse OOD noises, including synthetic noise, real-world sRGB noise, and low-dose CT noise, demonstrate the superiority of our method.

Acknowledgment. This work was supported in part by the National Natural Science Foundation of China (NNSFC), under Grant Nos. 61672253 and 62071197.

References

- [1] Abdelrahman Abdelhamed, Stephen Lin, and Michael S Brown. A high-quality denoising dataset for smartphone cameras. In *Proceedings of the IEEE conference on computer vision and pattern recognition*, pages 1692–1700, 2018. 2, 5
- [2] Eirikur Agustsson and Radu Timofte. Ntire 2017 challenge on single image super-resolution: Dataset and study. In *The IEEE Conference on Computer Vision and Pattern Recognition (CVPR) Workshops*, 2017. 5
- [3] American Association of Physicists in Medicine. Low dose CT grand challenge. <https://www.aapm.org/grandchallenge/lowdosect/>, 2016. 5
- [4] Joshua Batson and Loic Royer. Noise2self: Blind denoising by self-supervision. In *International Conference on Machine Learning*, pages 524–533. PMLR, 2019. 2
- [5] Fei Chen, Lei Zhang, and Huimin Yu. External patch prior guided internal clustering for image denoising. In *Proceedings of the IEEE international conference on computer vision*, pages 603–611, 2015. 2
- [6] Haoyu Chen, Jinjin Gu, Yihao Liu, Salma Abdel Magid, Chao Dong, Qiong Wang, Hanspeter Pfister, and Lei Zhu. Masked image training for generalizable deep image denoising. In *Proceedings of the IEEE/CVF Conference on Computer Vision and Pattern Recognition*, pages 1692–1703, 2023. 1, 2, 5, 6, 7, 3
- [7] Hao Chen, Chenyuan Qu, Yu Zhang, Chen Chen, and Jianbo Jiao. Multi-view self-supervised disentanglement for general image denoising. In *Proceedings of the IEEE/CVF International Conference on Computer Vision*, pages 12281–12291, 2023. 1, 2
- [8] Xinlei Chen, Saining Xie, and Kaiming He. An empirical study of training self-supervised vision transformers. In *Proceedings of the IEEE/CVF International Conference on Computer Vision*, pages 9640–9649, 2021. 8
- [9] Jun Cheng, Tao Liu, and Shan Tan. Score priors guided deep variational inference for unsupervised real-world single image denoising. In *Proceedings of the IEEE/CVF International Conference on Computer Vision*, pages 12937–12948, 2023. 3
- [10] Kostadin Dabov, Alessandro Foi, Vladimir Katkovnik, and Karen Egiazarian. Image denoising by sparse 3-d transform-domain collaborative filtering. *IEEE Transactions on image processing*, 16(8):2080–2095, 2007. 4
- [11] Alexey Dosovitskiy, Lucas Beyer, Alexander Kolesnikov, Dirk Weissenborn, Xiaohua Zhai, Thomas Unterthiner, Mostafa Dehghani, Matthias Minderer, Georg Heigold, Sylvain Gelly, et al. An image is worth 16x16 words: Transformers for image recognition at scale. In *International Conference on Learning Representations*, 2020. 3
- [12] Wenchao Du, Hu Chen, and Hongyu Yang. Learning invariant representation for unsupervised image restoration. In *Proceedings of the IEEE/CVF conference on computer vision and pattern recognition*, pages 14483–14492, 2020. 1, 2, 5
- [13] Ben Fei, Zhaoyang Lyu, Liang Pan, Junzhe Zhang, Weidong Yang, Tianyue Luo, Bo Zhang, and Bo Dai. Generative diffusion prior for unified image restoration and enhancement. In *Proceedings of the IEEE/CVF Conference on Computer Vision and Pattern Recognition*, pages 9935–9946, 2023. 3
- [14] Rich Franzen. Kodak lossless true color image suite. <http://r0k.us/graphics/kodak/>, 1999. 5
- [15] Shi Guo, Zifei Yan, Kai Zhang, Wangmeng Zuo, and Lei Zhang. Toward convolutional blind denoising of real photographs. In *Proceedings of the IEEE/CVF conference on computer vision and pattern recognition*, pages 1712–1722, 2019. 5
- [16] Kaiming He, Xiangyu Zhang, Shaoqing Ren, and Jian Sun. Deep residual learning for image recognition. In *Proceedings of the IEEE conference on computer vision and pattern recognition*, pages 770–778, 2016. 3
- [17] Jia-Bin Huang, Abhishek Singh, and Narendra Ahuja. Single image super-resolution from transformed self-exemplars. In *Proceedings of the IEEE conference on computer vision and pattern recognition*, pages 5197–5206, 2015. 5
- [18] Tao Huang, Songjiang Li, Xu Jia, Huchuan Lu, and Jianzhuang Liu. Neighbor2neighbor: Self-supervised denoising from single noisy images. In *Proceedings of the IEEE/CVF conference on computer vision and pattern recognition*, pages 14781–14790, 2021. 1, 2
- [19] Junha Hyung, Sungwon Hwang, Daejin Kim, Hyunji Lee, and Jaegul Choo. Local 3d editing via 3d distillation of clip knowledge. In *Proceedings of the IEEE/CVF Conference on Computer Vision and Pattern Recognition*, pages 12674–12684, 2023. 1, 2
- [20] Zheyang Jin, Shiqi Chen, Yueting Chen, Zhihai Xu, and Hua-jun Feng. Let segment anything help image dehaze. *arXiv preprint arXiv:2306.15870*, 2023. 3
- [21] Bahjat Kawar, Gregory Vaksman, and Michael Elad. Snips: Solving noisy inverse problems stochastically. *Advances in Neural Information Processing Systems*, 34:21757–21769, 2021. 3
- [22] Bahjat Kawar, Michael Elad, Stefano Ermon, and Jiaming Song. Denoising diffusion restoration models. 2022. 3
- [23] Kwanyoung Kim and Jong Chul Ye. Noise2score: tweedie’s approach to self-supervised image denoising without clean images. *Advances in Neural Information Processing Systems*, 34:864–874, 2021. 2
- [24] Alexander Kirillov, Eric Mintun, Nikhila Ravi, Hanzi Mao, Chloe Rolland, Laura Gustafson, Tete Xiao, Spencer Whitehead, Alexander C Berg, Wan-Yen Lo, et al. Segment anything. *arXiv preprint arXiv:2304.02643*, 2023. 3
- [25] Simon Kornblith, Mohammad Norouzi, Honglak Lee, and Geoffrey Hinton. Similarity of neural network representations revisited. In *International conference on machine learning*, pages 3519–3529. PMLR, 2019. 2, 3
- [26] Alexander Krull, Tim-Oliver Buchholz, and Florian Jug. Noise2void-learning denoising from single noisy images. In *Proceedings of the IEEE/CVF conference on computer vision and pattern recognition*, pages 2129–2137, 2019. 1, 2
- [27] Christian Ledig, Lucas Theis, Ferenc Huszár, Jose Caballero, Andrew Cunningham, Alejandro Acosta, Andrew Aitken, Alykhan Tejani, Johannes Totz, Zehan Wang, et al. Photo-realistic single image super-resolution using a generative adversarial network. In *Proceedings of the IEEE conference on*

- computer vision and pattern recognition*, pages 4681–4690, 2017. 2
- [28] Wooseok Lee, Sanghyun Son, and Kyoung Mu Lee. Apbsn: Self-supervised denoising for real-world images via asymmetric pd and blind-spot network. In *Proceedings of the IEEE/CVF Conference on Computer Vision and Pattern Recognition*, pages 17725–17734, 2022. 1, 2
- [29] Pan Li, Da Li, Wei Li, Shaogang Gong, Yanwei Fu, and Timothy M Hospedales. A simple feature augmentation for domain generalization. In *Proceedings of the IEEE/CVF International Conference on Computer Vision*, pages 8886–8895, 2021. 4
- [30] Siwei Li, Mingxuan Liu, Yating Zhang, Shu Chen, Haoxiang Li, Hong Chen, and Zifei Dou. Sam-deblur: Let segment anything boost image deblurring. *arXiv preprint arXiv:2309.02270*, 2023. 3
- [31] Xuanlin Li, Yunhao Fang, Minghua Liu, Zhan Ling, Zhuowen Tu, and Hao Su. Distilling large vision-language model with out-of-distribution generalizability. In *ICCV*, pages 2492–2503, 2023. 1, 2
- [32] Xin Li, Bingchen Li, Xin Jin, Cuiling Lan, and Zhibo Chen. Learning distortion invariant representation for image restoration from a causality perspective. In *Proceedings of the IEEE/CVF Conference on Computer Vision and Pattern Recognition*, pages 1714–1724, 2023. 1, 2, 5, 6, 7, 3
- [33] Yawei Li, Yuchen Fan, Xiaoyu Xiang, Denis Demandolx, Rakesh Ranjan, Radu Timofte, and Luc Van Gool. Efficient and explicit modelling of image hierarchies for image restoration. In *Proceedings of the IEEE/CVF Conference on Computer Vision and Pattern Recognition*, pages 18278–18289, 2023. 1, 2, 3
- [34] Feng Liang, Bichen Wu, Xiaoliang Dai, Kunpeng Li, Yinan Zhao, Hang Zhang, Peizhao Zhang, Peter Vajda, and Diana Marculescu. Open-vocabulary semantic segmentation with mask-adapted clip. In *Proceedings of the IEEE/CVF Conference on Computer Vision and Pattern Recognition*, pages 7061–7070, 2023. 1, 2
- [35] Jingyun Liang, Jie Zhang Cao, Guolei Sun, Kai Zhang, Luc Van Gool, and Radu Timofte. Swinir: Image restoration using swin transformer. In *2021 IEEE/CVF International Conference on Computer Vision Workshops (ICCVW)*, pages 1833–1844. IEEE Computer Society, 2021. 2, 3
- [36] Ilya Loshchilov and Frank Hutter. Decoupled weight decay regularization. In *International Conference on Learning Representations*, 2018. 5
- [37] Zhihe Lu, Zeyu Xiao, Jiawang Bai, Zhiwei Xiong, and Xinchao Wang. Can sam boost video super-resolution? *arXiv preprint arXiv:2305.06524*, 2023. 3
- [38] Huaishao Luo, Junwei Bao, Youzheng Wu, Xiaodong He, and Tianrui Li. Segclip: Patch aggregation with learnable centers for open-vocabulary semantic segmentation. In *International Conference on Machine Learning*, pages 23033–23044. PMLR, 2023. 2
- [39] Ziwei Luo, Fredrik K Gustafsson, Zheng Zhao, Jens Sjölund, and Thomas B Schön. Controlling vision-language models for universal image restoration. *arXiv preprint arXiv:2310.01018*, 2023. 3
- [40] David Martin, Charless Fowlkes, Doron Tal, and Jitendra Malik. A database of human segmented natural images and its application to evaluating segmentation algorithms and measuring ecological statistics. In *Proceedings Eighth IEEE International Conference on Computer Vision. ICCV 2001*, pages 416–423. IEEE, 2001. 5
- [41] Sreyas Mohan, Zahra Kadkhodaie, Eero P Simoncelli, and Carlos Fernandez-Granda. Robust and interpretable blind image denoising via bias-free convolutional neural networks. In *International Conference on Learning Representations*, 2019. 1, 2
- [42] Sreyas Mohan, Joshua L Vincent, Ramon Manzorro, Peter Crozier, Carlos Fernandez-Granda, and Eero Simoncelli. Adaptive denoising via gaintuning. *Advances in neural information processing systems*, 34:23727–23740, 2021. 2
- [43] Seonghyeon Nam, Youngbae Hwang, Yasuyuki Matsushita, and Seon Joo Kim. A holistic approach to cross-channel image noise modeling and its application to image denoising. In *Proceedings of the IEEE conference on computer vision and pattern recognition*, pages 1683–1691, 2016. 5
- [44] Reyhaneh Neshatavar, Mohsen Yavartanoo, Sanghyun Son, and Kyoung Mu Lee. Cvf-sid: Cyclic multi-variate function for self-supervised image denoising by disentangling noise from image. In *Proceedings of the IEEE/CVF Conference on Computer Vision and Pattern Recognition*, pages 17583–17591, 2022. 1, 2, 6, 7
- [45] Chuang Niu, Mengzhou Li, Fenglei Fan, Weiwen Wu, Xiaodong Guo, Qing Lyu, and Ge Wang. Noise suppression with similarity-based self-supervised deep learning. *IEEE Transactions on Medical Imaging*, 42(6):1590–1602, 2023. 7
- [46] Tongyao Pang, Huan Zheng, Yuhui Quan, and Hui Ji. Recorrupted-to-recorrupted: unsupervised deep learning for image denoising. In *Proceedings of the IEEE/CVF conference on computer vision and pattern recognition*, pages 2043–2052, 2021. 2
- [47] Adam Paszke, Sam Gross, Francisco Massa, Adam Lerer, James Bradbury, Gregory Chanan, Trevor Killeen, Zeming Lin, Natalia Gimelshein, Luca Antiga, et al. Pytorch: An imperative style, high-performance deep learning library. *Advances in neural information processing systems*, 32, 2019. 5
- [48] Alec Radford, Jong Wook Kim, Chris Hallacy, Aditya Ramesh, Gabriel Goh, Sandhini Agarwal, Girish Sastry, Amanda Askell, Pamela Mishkin, Jack Clark, et al. Learning transferable visual models from natural language supervision. In *International conference on machine learning*, pages 8748–8763. PMLR, 2021. 1, 2
- [49] Yongming Rao, Wenliang Zhao, Guangyi Chen, Yansong Tang, Zheng Zhu, Guan Huang, Jie Zhou, and Jiwen Lu. Denseclip: Language-guided dense prediction with context-aware prompting. In *Proceedings of the IEEE/CVF Conference on Computer Vision and Pattern Recognition*, pages 18082–18091, 2022. 1, 2
- [50] Chitwan Saharia, Jonathan Ho, William Chan, Tim Salimans, David J Fleet, and Mohammad Norouzi. Image super-resolution via iterative refinement. *IEEE Transactions*

- on *Pattern Analysis and Machine Intelligence*, 45(4):4713–4726, 2022. 2
- [51] Zheyang Shen, Jiashuo Liu, Yue He, Xingxuan Zhang, Renzhe Xu, Han Yu, and Peng Cui. Towards out-of-distribution generalization: A survey. *arXiv preprint arXiv:2108.13624*, 2021. 1
- [52] Yang Song, Liyue Shen, Lei Xing, and Stefano Ermon. Solving inverse problems in medical imaging with score-based generative models. In *International Conference on Learning Representations*, 2022. 7
- [53] Laurens Van der Maaten and Geoffrey Hinton. Visualizing data using t-sne. *Journal of machine learning research*, 9(11), 2008. 4
- [54] Zichun Wang, Ying Fu, Ji Liu, and Yulun Zhang. Lg-bpn: Local and global blind-patch network for self-supervised real-world denoising. In *Proceedings of the IEEE/CVF Conference on Computer Vision and Pattern Recognition*, pages 18156–18165, 2023. 1, 2
- [55] Kan Wu, Houwen Peng, Zhenghong Zhou, Bin Xiao, Mengchen Liu, Lu Yuan, Hong Xuan, Michael Valenzuela, Xi Stephen Chen, Xinggong Wang, et al. Tinyclip: Clip distillation via affinity mimicking and weight inheritance. In *Proceedings of the IEEE/CVF International Conference on Computer Vision*, pages 21970–21980, 2023. 2
- [56] Zeyu Xiao, Jiawang Bai, Zhihe Lu, and Zhiwei Xiong. A dive into sam prior in image restoration. *arXiv preprint arXiv:2305.13620*, 2023. 3
- [57] Jun Xu, Hui Li, Zhetong Liang, David Zhang, and Lei Zhang. Real-world noisy image denoising: A new benchmark. *arXiv preprint arXiv:1804.02603*, 2018. 5
- [58] Hanshu Yan, Jingfeng Zhang, Jiashi Feng, Masashi Sugiyama, and Vincent Y. F. Tan. Towards adversarially robust deep image denoising. In *Proceedings of the Thirty-First International Joint Conference on Artificial Intelligence, IJCAI-22*, pages 1516–1522, 2022. 1, 2, 5, 6, 7, 3
- [59] Lijun Yu, Yong Cheng, Zhiruo Wang, Vivek Kumar, Wolfgang Macherey, Yanping Huang, David A Ross, Irfan Essa, Yonatan Bisk, Ming-Hsuan Yang, et al. Spae: Semantic pyramid autoencoder for multimodal generation with frozen llms. *arXiv preprint arXiv:2306.17842*, 2023. 3
- [60] Syed Waqas Zamir, Aditya Arora, Salman Khan, Munawar Hayat, Fahad Shahbaz Khan, and Ming-Hsuan Yang. Restormer: Efficient transformer for high-resolution image restoration. *arXiv preprint arXiv:2111.09881*, 2021. 1, 2, 3, 5, 6
- [61] Syed Waqas Zamir, Aditya Arora, Salman Khan, Munawar Hayat, Fahad Shahbaz Khan, Ming-Hsuan Yang, and Ling Shao. Multi-stage progressive image restoration. In *Proceedings of the IEEE/CVF Conference on Computer Vision and Pattern Recognition*, pages 14821–14831, 2021. 3
- [62] Kai Zhang, Wangmeng Zuo, Yunjin Chen, Deyu Meng, and Lei Zhang. Beyond a gaussian denoiser: Residual learning of deep cnn for image denoising. *IEEE transactions on image processing*, 26(7):3142–3155, 2017. 1, 2, 5, 6, 3
- [63] Kai Zhang, Yawei Li, Wangmeng Zuo, Lei Zhang, Luc Van Gool, and Radu Timofte. Plug-and-play image restoration with deep denoiser prior. *IEEE Transactions on Pattern Analysis and Machine Intelligence*, 44(10):6360–6376, 2021. 1, 2, 3
- [64] Lei Zhang, Xiaolin Wu, Antoni Buades, and Xin Li. Color demosaicking by local directional interpolation and nonlocal adaptive thresholding. *Journal of Electronic imaging*, 20(2):023016–023016, 2011. 5
- [65] Renrui Zhang, Ziyao Zeng, Ziyu Guo, and Yafeng Li. Can language understand depth? In *Proceedings of the 30th ACM International Conference on Multimedia*, pages 6868–6874, 2022. 1
- [66] Y Zhang, K Li, B Zhong, and Y Fu. Residual non-local attention networks for image restoration. In *International Conference on Learning Representations*, 2019. 2
- [67] Hang Zhao, Orazio Gallo, Iuri Frosio, and Jan Kautz. Loss functions for image restoration with neural networks. *IEEE Transactions on computational imaging*, 3(1):47–57, 2016. 2
- [68] Dihan Zheng, Xiaowen Zhang, Kaisheng Ma, and Chenglong Bao. Learn from unpaired data for image restoration: A variational bayes approach. *IEEE Transactions on Pattern Analysis and Machine Intelligence*, 2022. 6, 7
- [69] Chong Zhou, Chen Change Loy, and Bo Dai. Extract free dense labels from clip. In *European Conference on Computer Vision*, pages 696–712. Springer, 2022. 1, 2
- [70] Kaiyang Zhou, Ziwei Liu, Yu Qiao, Tao Xiang, and Chen Change Loy. Domain generalization: A survey. *IEEE Transactions on Pattern Analysis and Machine Intelligence*, 2022. 1
- [71] Ziqin Zhou, Yinjie Lei, Bowen Zhang, Lingqiao Liu, and Yifan Liu. Zegclip: Towards adapting clip for zero-shot semantic segmentation. In *Proceedings of the IEEE/CVF Conference on Computer Vision and Pattern Recognition*, pages 11175–11185, 2023. 1, 2
- [72] Yuanzhi Zhu, Kai Zhang, Jingyun Liang, Jiezhang Cao, Bihan Wen, Radu Timofte, and Luc Van Gool. Denoising diffusion models for plug-and-play image restoration. In *Proceedings of the IEEE/CVF Conference on Computer Vision and Pattern Recognition*, pages 1219–1229, 2023. 3

Transfer CLIP for Generalizable Image Denoising

Supplementary Material

Algorithm 1 Extract dense features from CLIP ResNet.

```

# PyTorch code of CLIP ResNet image encoder
# the forward function
def forward(self, x):
    out = [] # store multi-scale dense features
    x = x.type(self.conv1.weight.dtype)
    x = self.relu1(self.bn1(self.conv1(x)))
    x = self.relu2(self.bn2(self.conv2(x)))
    x = self.relu3(self.bn3(self.conv3(x)))
    out.append(x) # scale-1 F1
    x = self.avgpool(x)
    x = self.layer1(x); out.append(x) # scale-2 F2
    x = self.layer2(x); out.append(x) # scale-3 F3
    x = self.layer3(x); out.append(x) # scale-4 F4
    x = self.layer4(x); out.append(x) # scale-5 F5
    x = self.attnpool(x)
    return out

```

7. More Analyses of CLIP ResNet Encoder

We conduct more feature analysis of CLIP frozen ResNet encoder for the image *Lena* using Poisson noise and CKA similarity measure, respectively, and report the results in Fig. 9 and 10. Besides, feature similarity analysis of CLIP ResNet encoder for the image *flowers* from Set14 is also performed and shown in Fig. 11.

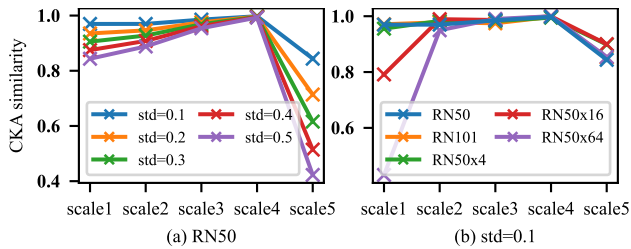


Figure 9. Feature similarity analysis of the CLIP ResNet encoder under *i.i.d.* Gaussian noise with varying levels and CKA similarity measure

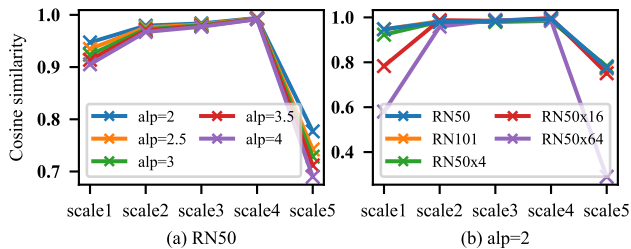


Figure 10. Feature similarity analysis of the CLIP ResNet image encoder under Poisson noise with varying levels and cosine similarity measure

8. More Implementation Details

We present the details of our learnable decoder in Fig. 12.

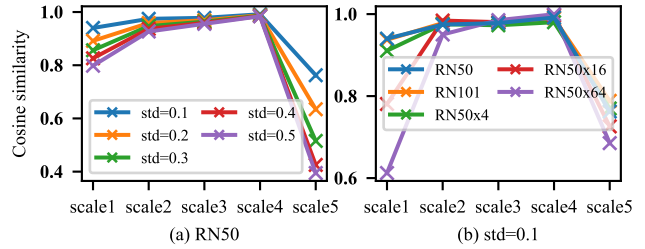


Figure 11. Feature similarity analysis for the image *flowers* from set14 under Gaussian noise and cosine similarity measure

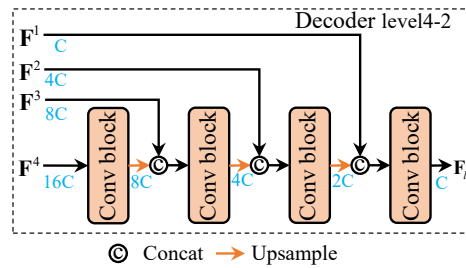


Figure 12. The detail of the learnable decoder (level-4 to -2) in our CLIPDenoising. The symbols with lightblue represent the channel number, where C is the base channel and is 64 in RN50

9. More experimental results

9.1. Model size and inference time

We provide the model size, inference time, and FLOPs of compared methods in Table 6. Note that the frozen RN50 (excluding the last layer) in our model has 8.5M parameters, and the learnable decoder has 11M parameters. And HAT uses the DnCNN model.

Table 6. Efficiency comparisons (test on size $3 \times 512 \times 512$)

	DnCNN	Restormer	MaskDeno.	HAT	DIL	ours
Params(M)	0.67	26.1	0.88	0.67	16.6	19.5
Infer.time(s)	0.034	0.415	2.239	0.034	0.867	0.018
FLOPs(G)	176.1	564.0	204.9	176.1	4360	83.58

9.2. Results on environmental noise

We consider image deraining task. We use Rain100L as the training set and use *Rain12*, *Rain drop (S)*, and *Rain and mist (S)* as OOD test sets. Results in Table 7 imply that our model exhibits better generalization capability than PromptIR (NeurIPS 2023), a recent image restoration model.

9.3. Results of using CLIP ViT image encoder

We incorporate CLIP ViT-B/16 image encoder into our model and report the resultant results in Table 8. Specifically, the model ex-

Table 7. Results on image deraining tasks (PSNR/SSIM)

	<i>Rain12</i>	<i>Rain drop (S)</i>	<i>Rain and mist (S)</i>
PromptIR	35.00/0.944	22.98/0.835	21.89/0.673
ours	35.11/0.953	23.66/0.838	28.56/0.869

tracts features from the middle (i.e., 7-th) layer of the frozen ViT-B/16, and then feeds it to 4 learnable ViT blocks and 4 learnable upsampling blocks that upsample the deep features back to the original image space. By comparing Table 8 and Tables 1, 9, our model with image ViT encoder shows inferior in-distribution and OOD performance.

Table 8. Results of using CLIP ViT-B/16 image encoder

	Gauss(15)	Gauss(50)	Poisson(3.5)	Speckle(0.04)
McM	33.28/0.903	21.29/0.372	24.78/0.618	27.41/0.755
Kodak24	33.98/0.914	20.59/0.338	24.02/0.529	28.08/0.741

10. Experiments on MoCo-v3 ResNet50

We conduct the feature similarity analysis of frozen MoCo-v3 ResNet50 for the image *Lena* using *i.i.d.* Gaussian noise and cosine similarity measure, and report the result in Fig. 13. Five multi-scale features show robustness to noise. Subsequently, we substitute the RN50 of CLIP with the RN50 of MoCo-v3 in our denoiser and perform the model training and OOD experiments. As observed in Table 10, frozen MoCo-v3 RN50-powered deep denoiser exhibits a certain level of generalization ability compared with DnCNN and our method.

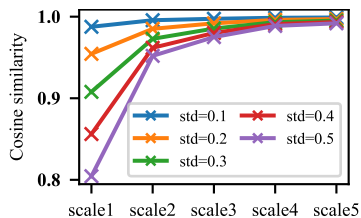


Figure 13. Feature similarity analysis of the MoCo-v3 ResNet50 under Gaussian noise. Cosine similarity is utilized here

Table 9. Additional quantitative comparison of different methods on CBSD68, McMaster, Kodak24 and Urban100 datasets with regard to diverse synthetic OOD noises. The best results are highlighted in **bold** and the second best is underlined. Note that *multiple noise levels* are required by HAT and DIL during the training to achieve generalization, while our method only needs *one noise level* for training

Noise Types	Datasets	DnCNN [62]	Restormer [60]	MaskDenoising [6]	HAT [58]	DIL [32]	Ours
Gauss $\sigma = 15$	CBSD68	<u>33.78/0.931</u>	34.42/0.936	30.99/0.888	33.22/0.912	32.50/0.906	<u>33.97/0.930</u>
	McMaster	<u>34.03/0.914</u>	35.61/0.935	30.85/0.832	33.04/0.883	32.45/0.853	<u>33.86/0.910</u>
	Kodak24	<u>34.59/0.924</u>	35.49/0.931	31.79/0.884	33.88/0.905	33.37/0.912	<u>34.69/0.922</u>
	Urban100	<u>32.10/0.934</u>	34.57/0.955	29.50/0.899	32.48/0.916	32.15/0.920	<u>33.15/0.930</u>
Gauss $\sigma = 25$	CBSD68	29.89/0.828	27.21/0.681	28.44/0.815	<u>30.54/0.853</u>	29.98/0.843	31.02/0.878
	McMaster	30.46/0.806	27.31/0.633	28.76/0.778	<u>30.41/0.807</u>	30.17/0.790	31.50/0.866
	Kodak24	30.53/0.808	27.64/0.639	29.08/0.792	<u>31.37/0.849</u>	30.99/0.856	31.86/0.871
	Urban100	28.88/0.847	27.35/0.744	27.63/0.836	<u>29.97/0.867</u>	29.72/0.876	30.72/0.893
Spatial Gauss $\sigma = 45$	CBSD68	28.05/0.785	24.51/0.668	28.19/0.815	<u>28.33/0.791</u>	26.33/0.703	29.43/0.849
	McMaster	28.24/0.740	24.01/0.539	<u>28.27/0.762</u>	28.44/0.742	26.47/0.646	29.82/0.825
	Kodak24	28.23/0.752	23.66/0.609	<u>28.85/0.805</u>	28.44/0.760	26.31/0.652	30.12/0.838
	Urban100	27.53/0.806	25.80/0.722	<u>27.34/0.837</u>	28.32/0.809	26.51/0.737	29.42/0.868
Spatial Gauss $\sigma = 50$	CBSD68	26.92/0.741	23.98/0.630	<u>27.47/0.790</u>	27.32/0.752	25.43/0.665	28.51/0.825
	McMaster	27.16/0.693	24.63/0.573	<u>27.60/0.738</u>	27.49/0.703	25.61/0.609	29.10/0.803
	Kodak24	27.04/0.702	23.29/0.569	<u>28.09/0.778</u>	27.37/0.715	25.39/0.611	29.21/0.815
	Urban100	26.49/0.766	24.93/0.690	<u>26.74/0.815</u>	27.36/0.776	25.61/0.704	28.55/0.847
Poisson $\alpha = 2.5$	CBSD68	28.70/0.806	25.63/0.693	27.80/0.806	30.15/0.858	<u>29.53/0.870</u>	<u>29.94/0.874</u>
	McMaster	29.80/0.799	25.75/0.693	28.55/0.730	<u>30.87/0.840</u>	30.74/0.871	30.93/0.864
	Kodak24	29.23/0.776	26.06/0.644	28.42/0.781	30.90/0.843	30.42/0.868	30.93/0.869
	Urban100	27.56/0.806	25.14/0.719	26.95/0.815	29.52/0.871	29.17/0.893	<u>29.51/0.884</u>
Poisson $\alpha = 3$	CBSD68	26.37/0.712	23.55/0.615	25.87/0.718	28.48/0.804	<u>28.52/0.844</u>	28.71/0.846
	McMaster	27.49/0.720	23.62/0.632	26.13/0.667	29.30/0.784	<u>29.78/0.848</u>	29.82/0.843
	Kodak24	26.68/0.660	23.95/0.561	27.04/0.683	29.16/0.779	<u>29.45/0.844</u>	29.71/0.841
	Urban100	25.41/0.721	22.72/0.642	25.33/0.737	27.82/0.815	<u>28.09/0.874</u>	28.27/0.862
Speckle $\sigma^2 = 0.02$	CBSD68	31.79/0.898	29.10/0.826	29.91/0.875	32.50/0.916	31.57/0.924	<u>31.82/0.904</u>
	McMaster	32.74/0.886	28.89/0.800	30.47/0.809	33.11/0.899	<u>32.66/0.907</u>	<u>32.28/0.870</u>
	Kodak24	32.82/0.895	29.96/0.814	30.80/0.874	33.26/0.908	<u>32.35/0.919</u>	<u>32.91/0.908</u>
	Urban100	30.11/0.893	28.24/0.828	28.60/0.883	31.49/0.917	30.90/0.930	<u>30.94/0.904</u>
Speckle $\sigma^2 = 0.03$	CBSD68	30.10/0.856	26.78/0.765	28.99/0.851	31.10/0.893	30.40/0.906	<u>30.48/0.886</u>
	McMaster	31.21/0.846	26.81/0.752	29.70/0.778	31.95/0.873	<u>31.70/0.904</u>	31.31/0.858
	Kodak24	31.12/0.852	27.50/0.740	29.90/0.848	31.95/0.884	31.28/0.901	<u>31.64/0.891</u>
	Urban100	28.37/0.841	25.86/0.774	27.65/0.847	30.10/0.892	<u>29.72/0.916</u>	29.69/0.889
Speckle $\sigma^2 = 0.04$	CBSD68	28.65/0.812	25.13/0.719	27.94/0.815	29.97/0.867	<u>29.56/0.890</u>	<u>29.49/0.870</u>
	McMaster	29.69/0.804	25.30/0.717	28.68/0.736	30.90/0.845	30.94/0.893	<u>30.47/0.845</u>
	Kodak24	29.53/0.801	25.66/0.683	28.76/0.804	30.82/0.856	30.49/0.887	<u>30.67/0.876</u>
	Urban100	26.92/0.795	24.17/0.732	26.64/0.804	28.86/0.862	<u>28.82/0.903</u>	<u>28.69/0.875</u>
Salt&Pepper $\alpha = 0.012$	CBSD68	28.56/0.814	25.88/0.779	30.49/0.863	29.31/0.846	<u>30.81/0.865</u>	31.95/0.890
	McMaster	27.76/0.773	25.32/0.746	30.11/0.798	28.39/0.804	<u>30.44/0.820</u>	31.90/0.863
	Kodak24	29.17/0.797	26.17/0.751	31.27/0.861	29.91/0.834	31.24/0.851	32.72/0.882
	Urban100	27.40/0.823	25.73/0.815	29.08/0.880	28.60/0.851	30.49/0.875	31.50/0.901
Salt&Pepper $\alpha = 0.016$	CBSD68	27.45/0.780	24.57/0.726	<u>30.13/0.853</u>	28.32/0.813	30.02/0.841	30.85/0.857
	McMaster	26.61/0.730	24.00/0.687	29.70/0.786	27.37/0.763	<u>29.75/0.793</u>	30.85/0.838
	Kodak24	28.05/0.760	24.81/0.690	<u>30.94/0.853</u>	28.95/0.797	30.52/0.827	31.67/0.863
	Urban100	26.42/0.806	24.45/0.771	28.76/0.871	27.63/0.820	<u>29.75/0.855</u>	30.30/0.889

Table 10. Quantitative comparison of DnCNN, our model with frozen CLIP RN50, and our model with frozen MoCo-v3 RN50 on McMaster and Kodak24 datasets with regard to various synthetic OOD noises. All methods are trained under *i.i.d.* Gaussian noise with $\sigma = 15$. Progressive feature augmentation is not used here.

	McMaster	Gauss $\sigma = 50$	Spatial Gauss $\sigma = 55$	Poisson $\alpha = 3.5$	Speckle $\sigma^2 = 0.04$	S&P $d = 0.02$
DnCNN		20.18/0.312	26.18/0.649	25.50/0.651	29.69/0.804	25.72/0.691
Ours+CLIP RN50		26.95/0.698	28.24/0.771	28.82/0.814	30.29/0.824	<u>29.62/0.795</u>
Ours+MoCo-v3 RN50		<u>24.85/0.625</u>	<u>27.36/0.748</u>	<u>26.92/0.747</u>	29.68/0.823	29.96/0.809
	Kodak24	Gauss $\sigma = 50$	Spatial Gauss $\sigma = 55$	Poisson $\alpha = 3.5$	Speckle $\sigma^2 = 0.04$	S&P $d = 0.02$
DnCNN		19.78/0.301	25.98/0.653	24.49/0.560	29.53/0.801	27.10/0.723
Ours+CLIP RN50		26.87/0.692	28.19/0.781	29.74/0.840	30.60/0.871	<u>30.52/0.832</u>
Ours+MoCo-v3 RN50		<u>25.59/0.630</u>	<u>27.72/0.747</u>	<u>26.82/0.718</u>	29.90/0.829	30.95/0.834

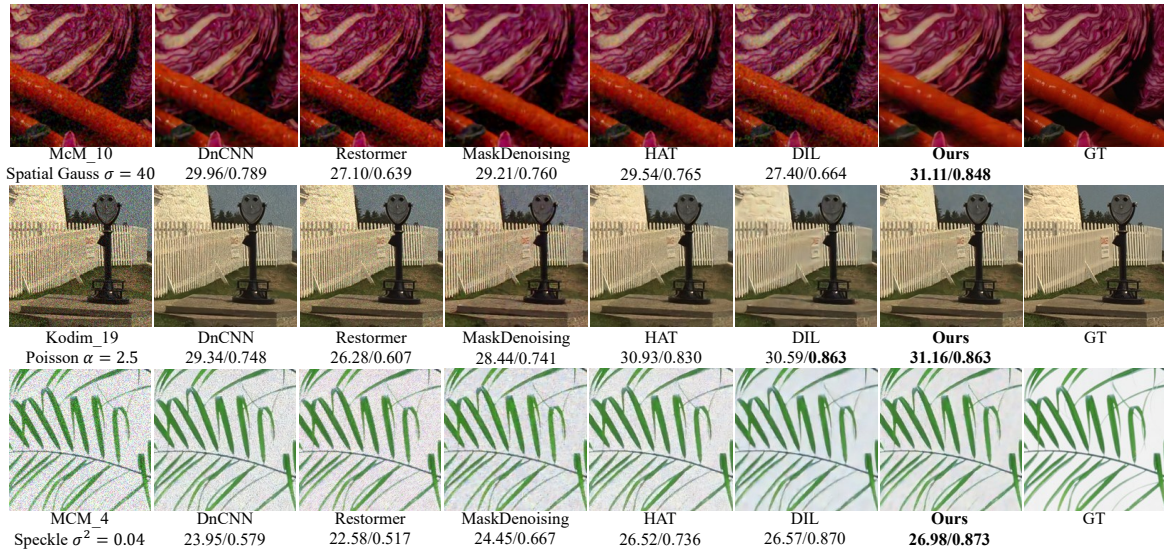


Figure 14. More qualitative denoising results on synthetic OOD noise.

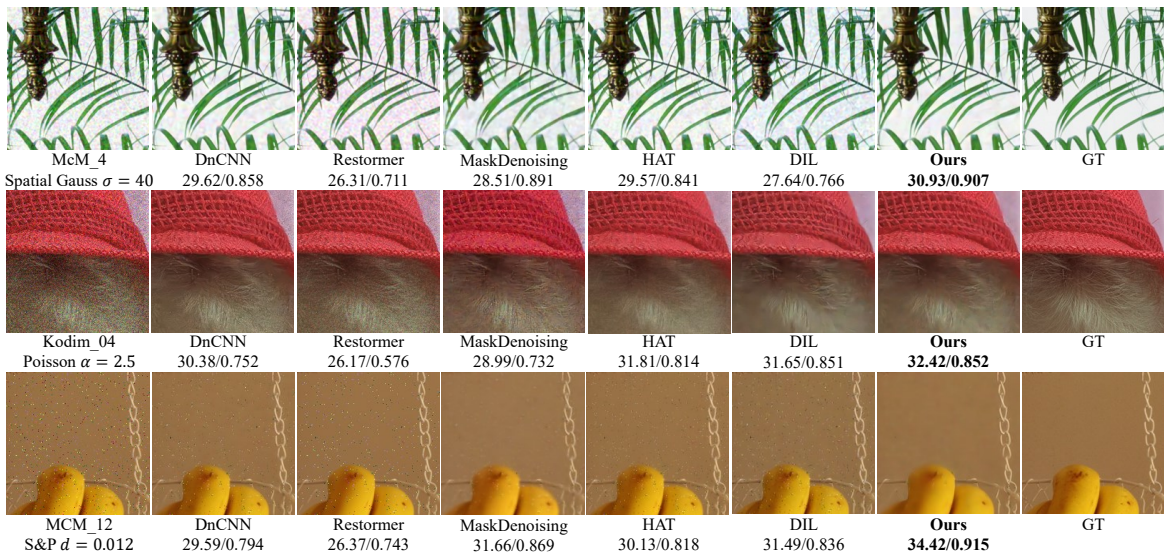


Figure 15. More qualitative denoising results on synthetic OOD noise.

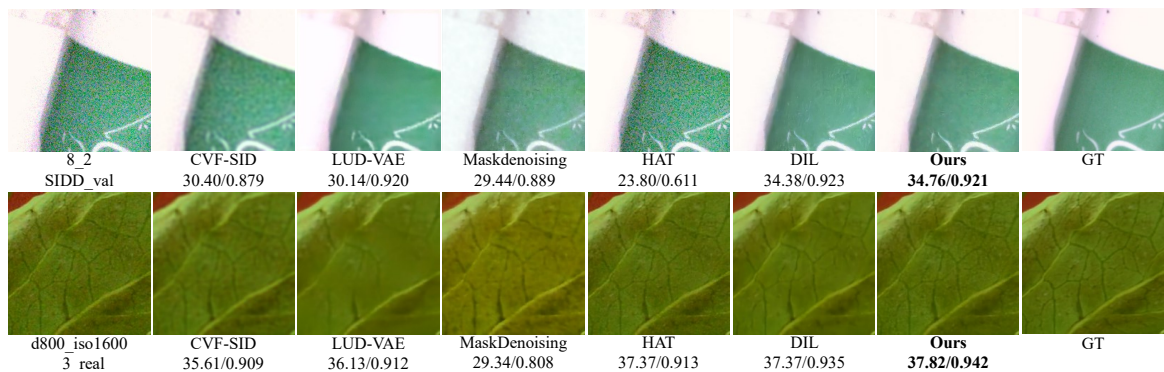


Figure 16. More qualitative denoising results on real-world sRGB noise